Advanced Journal of Chemistry-Section B
Natural Products and Medical Chemistry

Journal homepage: http://www.ajchem-b.com/

Original Research Article

Computational Studies on the Corrosion Inhibition of Mild Steel Using Pyrimidine Derivatives

Fater Iorhuna*, Abdullahi Muhammad Ayuba, and Abdulfatah Shehu Muhammad
Department of Pure and Industrial Chemistry, Faculty of Physical Sciences, Bayero University Kano, Nigeria

ARTICLE INFO

Article history
Submitted: 2023-05-19
Revised: 2023-06-20
Accepted: 2023-06-29
Available online: 2023-07-29
Manuscript ID: AJCB-2305-1173
DOI: 10.48309/ajcb.2023.398019.1173

KEYWORDS
Fukui Indices
Binding Energy
Geometric Optimization
Quantum Chemical Parameters
Physisorption

ABSTRACT

Quantum chemical parameters and molecular dynamic simulation studies were used to evaluate the corrosion inhibition of mild steel using pyrimidine derivatives (5-Phenoxy-6-phenyl-4-p-tolyl-1H-pyrimidin-2-one (***PMO***), 5-(7-Oxa-bicyclo[4.1.0]hepta-1(6),2,4-trien-2-yloxy)-pyrimidine-2,4-diamine (***PMA***), and 5-Phenoxy-6-phenyl-4-p-tolyl-1H-pyrimidine-2-thione (***PMS***)) as inhibitors. The pyrimidine derivatives were geometrically optimized using DFT with a restricted spin polarization, DNP basis set, and a local density function B3LYP. According to the local or global reactivity parameters investigated, including the energy gap (ΔE), dipole moment (μ), electronegativity (χ), global hardness (η), global electrophilicity index (ω), nucleophilicity (ε), energy of back donation ($\Delta E_{b\text{-}d}$), and fraction of electron transfer (ΔN) between the inhibitor molecule and the iron surface, PMS is relatively a better inhibitor on Fe(111) surface than other inhibitors studied. This is demonstrated by its higher nucleophilicity. According to the evaluated Fukui indices, the interaction point between molecules and Fe(111) surface involve heteroatoms of sulphur, oxygen, and nitrogen that donate electrons which are wholly nucleophilic in nature. The nature and strength of the compounds' adsorption on the Fe(111) surface was described by quenched molecular dynamics simulations in the following order: PMS>PMO>PMA. There is relatively a weak interaction for the studied molecules with the Fe(111) surface, according to the measured molecular bond lengths and angles before and after adsorption and as well as the calculated adsorption/binding energies. It is suggested that physical adsorption mechanism can be used to describe the nature of the interaction of the pyrimidine derivative molecules with the Fe (111) surface.

* Corresponding author: Iorhuna Fater
✉ E-mail: uyerfater22@gmail.com

GRAPHICAL ABSTRACT

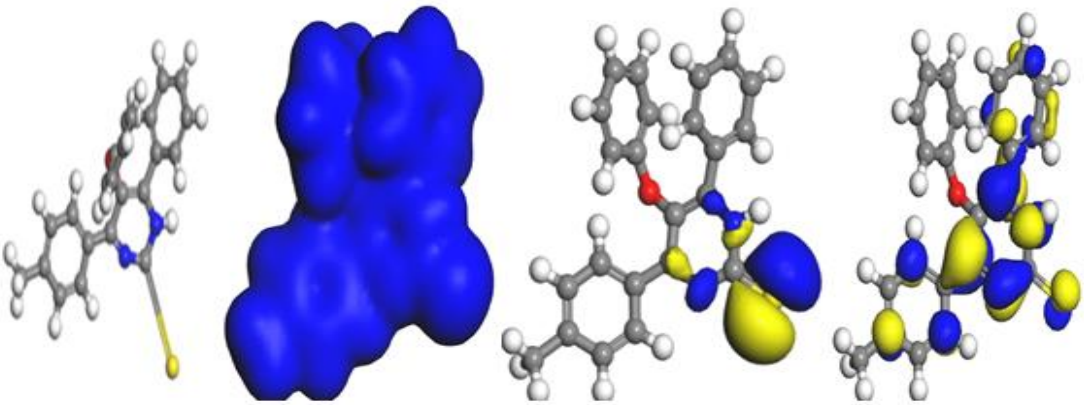

1- Introduction

One of the negative impacts of oxidation, which transforms pure refined metals into their ore states, is corrosion [1-4]. For the untrained personnel, corrosion appears as red blotches on the surface of iron metal, regardless of whether it also affects other metals [5]. When exposed to harsh environmental conditions, mild steel, a ferrous metal with a high proportion of iron and low carbon content, and its alloys undergo corrosion [6]. Similar to the other valuable metals like aluminum, zinc, and copper among others, this metal and its alloys find extensive applications in industry, automobile, building, and other materials used in day-to-day activities. Various techniques have been employed to stop this threat in the search for a solution to completely eliminate or significantly reduce the impact of corrosion on mild steel [7].

Recent years have seen a rise in the usage of eco-friendly chemicals that are cheap, efficient, and readily available as metal corrosion inhibitors [8-9]. Density functional theory (DFT) is one of the computational techniques used to theoretically solve chemistry-related problems since the development of computer software. These include studies on corrosion inhibition using different methods including the evaluation of quantum chemical parameters, molecular dynamic simulations, quantity structure activity relationship, and modeling which are now receiving the greatest attention [3-4, 10-11].

It is known that the majority of the organic metal corrosion inhibitors described in the literature contain various functional groups, heteroatoms, or polar atoms like sulphur, nitrogen, oxygen, and phosphorus.

Due to the lone pair of electrons found on these atoms, these molecules have both the highest occupied molecular orbital (HOMO) and the lowest unoccupied molecular orbital (LUMO) centers for donating and accepting electrons with metal surfaces [12]. These molecules are reported to have an adsorptive ability that prevents metallic materials from losing an electron from its d-orbitals and forming oxide, which leads to corrosion, but instead forms an association with the metal to successfully stop the corrosion process [7,10]. In this study, derivatives of pyrimidine such as: 5-Phenoxy-6-phenyl-4-p-tolyl-1H-pyrimidin-2-one (***PMO***), 5-(7-Oxa-bicyclo[4.1.0]hepta-1(6),2,4-trien-2-yloxy)-pyrimidine-2,4-diamine (***PMA***), and 5-Phenoxy-6-phenyl-4-p-tolyl-1H-pyrimidine-2-thione (***PMS***) were studied theoretically. The investigations led to the usage of these compound (PMS, PMA, and PMO) for the suppression of mild steel corrosion.

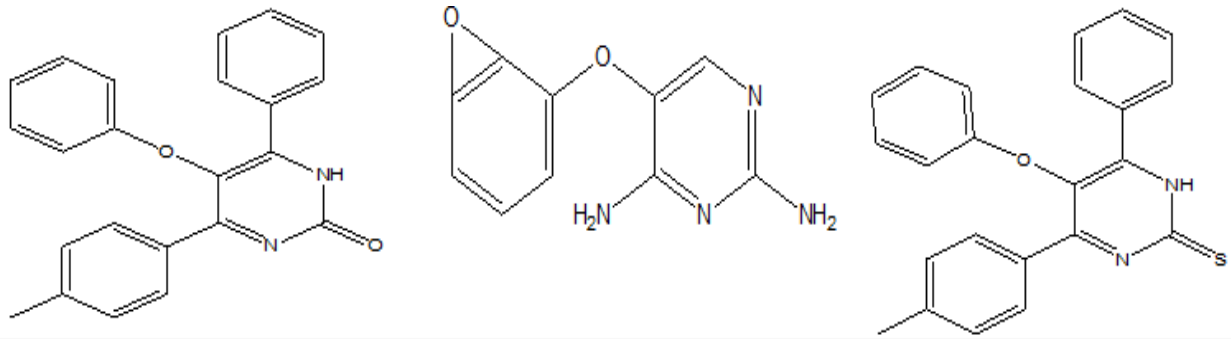

5-Phenoxy-6-phenyl-4-p-tolyl-1H-pyrimidin-2-one (PMO) | 5-(7-Oxa-bicyclo[4.1.0]hepta-1(6),2,4-trien-2-yloxy)-pyrimidine-2,4-diamine(PMA) | 5-Phenoxy-6-phenyl-4-p-tolyl-1H-pyrimidine-2-thione (PMS)

Fig.1 Molecular structure of the studied pyrimidine derivatives

Finding a credible explanation for the corrosion inhibition process of the studied compounds on Fe (111) surface is the goal of this research [27]. The molecules of the examined phytochemicals are displayed in Figure 1.

2- Methods

2-1 Sketching of the Studied Molecules

The 2D pyrimidine derivative molecular structures were sketched using Chem Draw Ultra 7.0.3 from CambridgeSoft and optimized using DMol³, a tool included in the BIOVIA Materials Studio 8.0 program from Accelrys, Inc. This is to ensure that the molecules had a stable geometry and used the least amount of energy possible. Before establishing the stable geometry of the pyrimidine derivative structures, the molecules imported from ChemDraw Ultra 7.0.3 CambridgeSoft to BIOVIA Materials studio 8.0 (Accelrys, Inc.) were optimized using the following settings: the local density function B3LYP using DFT-D under restricted spin polarization DNP basis and was set in aqueous phase [12-13].

2-2- Quantum Chemical Parameters Calculations

The quantum chemical calculation was performed using a DMol³ module in the BIOVIA Material Studio 8.0 program (Accelrys, Inc.) with underlying fundamentals of Density Functional Theory (DFT). The B3LYP function was used to calculate the parameters with the basis set to "double-numeric plus polarization" (DNP) in the aqueous phase model. Calculations were made to determine the ionization energy (IE), electron affinity (AE), and the other functions that define the reaction behaviours of molecules. In addition, determined were global reactivity parameters like electronegativity (χ) and electrophilicity (ω), which reflect the stability (energy) of the system when it becomes saturated by additional electron(s) from the environment.

Three global indices that describe a molecule's reactivity are global hardness (η), chemical potential (μ), and softness (σ). Global hardness (η), also known as resistance to charge transfer, chemical potential (μ), and softness (σ) quantify a molecule's polarizability. According to the Koopman's extended theorem, the following Equations (1-11), which are in terms of the initial electron distribution in the molecule and local reactivity calculation of the Fukui function f(r) from ab-initio quantum chemistry:

IE: Ionization energy (eV) $IE = -E_{HOMO}$ (1)

AE: Electron affinity (eV) $AE = -E_{LUMO}$ (2)

ΔE_g: Energy gap (eV) $\Delta E_g = E_{LUMO} - E_{HOMO}$ (3)

χ: Absolute electronegativity (eV) $\chi = \frac{IE+AE}{2} = -\frac{(E_{HOMO} + E_{LUMO})}{2}$ (4)

η: Global hardness (eV) $\eta = \frac{IE-AE}{2} = \frac{(E_{LUMO} - E_{HOMO})}{2}$ (5)

σ: Global softness $(eV)^{-1}$ $\sigma = \frac{1}{\eta} = -\frac{2}{E_{HOMO} - E_{LUMO}}$ (6)

ω: Global electrophilicity index (eV) $\omega = \frac{\mu^2}{2\eta} = \frac{\chi^2}{2\eta}$ (7)

μ: Chemical potential (Debye) $\mu \approx -\frac{1}{2}(IE + AE) = \frac{1}{2}(E_{LUMO} + E_{HOMO})$ (8)

ε: Nucleophilicity $(eV)^{-1}$ $\varepsilon = \frac{1}{\omega}$ (9)

$\Delta E_{b\text{-}d}$: Energy of back donation $\Delta E_{b-d} = -\frac{\eta}{4} = \frac{1}{8}(E_{HOMO} - E_{LUMO})$ (10)

ΔN: Fraction of electron(s) transfer $\Delta N = \frac{\chi Fe - \chi Inh.}{2(\eta Fe + \eta Inh)}$ (11)

The electron donating (ω^-), electron accepting (ω^+) powers, and net electrophilicity of the molecules was defined as shown in Equations (12-14), respectively:

ω^-: Electron donating power (eV) $\omega^- = \frac{(3IE+AE)^2}{16(IE-AE)}$ (12)

ω^+: Electron accepting power (eV) $\omega^+ = \frac{(IE+3AE)^2}{16(IE-AE)}$ (13)

Δω: Net electrophilicity (eV) $\Delta\omega^{\pm} = \omega^+ - (-\omega^-) = \omega^+ + \omega^-$ (14)

ηFe and ηInh are the absolute hardness of Fe and the inhibitor molecule, while χFe and χinh acted as Eigen values for the absolute electronegativity of Fe and the inhibitor molecule, respectively. By assuming that for a metallic bulk IP=EA because they are softer than the neutral metallic atoms, a theoretical value for the electro-negativity of bulk iron was found as χFe = 7.0 eV and a global hardness of iron surface as ηFe = 0eV [3-4, 10].

Another global descriptor, the Fukui second function (f^2), also referred to as the dual descriptor Δf(k), is defined as the distinction between nucleophilic and electrophilic local Fukui functions. These functions also gauge the electrophilicity or nucleophilicity of molecules based on the atoms' Fukui behaviour [12].

Site k favours a nucleophilic assault if $f^2(r) > 0$, whereas site k prefers an electrophilic attack if $f^2(r) < 0$. This suggests that $f^2(r)$ functions as a selectivity index for nucleophilic or electrophilic assaults.

$f(k)^+ = qk(N+1) - qk(N)$ (for nucleophilic attack) (15)

$f(k)^- = qk(N) - qk(N-1)$ (for electrophilic attack) (16)

$f(k)^0 = \frac{qk(N+1) - qk(N-1)}{2}$ (for radical attack) (17)

$\Delta f(k) = f^+ - f^- = f^2$ (Fukui function) (18)

Where, N is the number of electrons in the molecule, N+1 is an anion with an electron added to the LUMO of the neutral molecule, and N-1 is a cation with an electron removed from the HOMO of the neutral molecule, qk is the gross charge of atom k in the molecule, which is the electron density at a point r in space around the molecule. The ground state geometry served

as the basis for all calculations. Using an atomic charge partitioning scheme, such as Mulliken population analysis in Equations, these functions were condensed to the nuclei of the atoms [3-4].

2-3- Molecular Dynamic Simulations

The examined pyrimidine derivatives were simulated using a high stability quench adsorption technique on a surface of tightly packed Fe (111) atoms. The simulation process used a FORCITE tool package built inside the BIOVIA Materials Studio 8.0 program (Accelrys, Inc.). To simulate a representative portion of the surface, calculations were performed using the condensed-phase optimized molecular potentials for atomistic simulation studies (COMPASS) force field tool and the Smart algorithm method in a simulation box measuring 17Å x 12Å x 28Å. With a fractional depth of 3.0 Å, the (111) plane was cleavage across the Fe crystal. Prior to optimizing the surfaces, the shape of the bottom layers was restricted to prevent edge effects brought on by the molecule's sizes. The surfaces were then expanded into a 5 x 4 supercell. A compromise between a system with too much kinetic energy, where the molecule desorbs from the surface, and a system with insufficient kinetic energy, where the molecule cannot move across the surface, was made by fixing the temperature at 350K. The NVE (microcanonical) ensemble was used to set the temperature with a time step of 1 fs and a simulation time of 5 ps. To determine the statistical values of the energies on the surfaces of the iron (111) crystal, the process was intended to quench every 250 steps in a total of 5000 cycles. The lowest energy interactions of the molecules were found using FORCITE geometry optimized geometries of the molecules and the Fe (111) surfaces [3-4, 10, 14].

Equations (19-20) were used to determine the adsorption and binding energies between the pyrimidine derivatives and the Fe (111) surface.

$$E_A = E_T - (E_I + E_S) \quad (19)$$

$$E_B = - E_A \quad (20)$$

Where, E_A is the adsorption energy, E_T is the combined energy of the molecule and the iron surface, E_S is the energy of the iron surface, E_I is the energy of the inhibitor molecule without the iron surface, and E_B is the binding energy [3-4, 10, 14].

3-Results and Discussion

3-1- Frontier Molecular Orbitals

One of the key methods for conducting computational chemistry is quantum chemical calculations. These calculations have opened the door for the identification of several reaction pathways that can be utilized to address significant chemistry issues. In corrosion investigations and assessment, the technique, density functional theory, aids in the discovery of novel inhibitor moieties [3-4, 1-12]. In one of our published articles, we noted that the electronic distribution of a molecule's orbitals, which controls the chemical behaviour of the majority of molecules, determines a molecule's chemical reactivity [15]. In terms of the interactions between these orbitals on the moieties coming into contact with the metal surface, the frontier orbital conceptualizes chemical bonding and reactivity [16-17].

Therefore, the nature of the molecular orbitals and their willingness to give and absorb electron(s) between the two entities determine a compound's ability to effectively adsorb on the surface of the metal [18]. This is necessary if the minimum geometry of the molecules is to be attained. Since the highest occupied molecular orbital (HOMO) and the lowest unoccupied molecular orbital (LUMO) are essential for the molecule's reactivity, electron transfer is the mechanism that regulates the adsorption of these molecules on the metal surfaces [16-17]. The optimal structure of the compounds under study, the total electron density as well as the

molecules' HOMO and LUMO orbitals, were depicted in Figure 2.

The molecules' adsorption can occur using the entire atoms of the molecule with the metals surface, which can effectively inhibit the corrosion of the metal [13]. This result is demonstrated in Figure 2. The electron density of the pyrimidines can be seen to cover the entire molecular moieties. Furthermore, the presence of the hetero atoms and the pi bonds in the region indicates that the pyrimidine moieties under study are capable of having high inhibition on the metal surface. Accordingly, literature has shown that the presence of the hetero atom and the pi bond in the molecules increases their ability to inhibit the iron metals surface [16-17].

While the LUMO zone denotes the region of the molecules' electron deficit, the HOMO region of a molecule has the largest ability to donate electrons from one species to another. Both HOMO and LUMO orbitals occur in the same location of the pyrimidine molecules discussed above [17]. This may be due to the heteroatom existing in the same region of the molecule as functional groups serving as withdrawing and donating groups. Therefore, the presence of HOMO in a region abundant in hetero atoms and pi-bonds is a certain sign that the molecules under study will be successful at inhibiting iron metal corrosion [15].

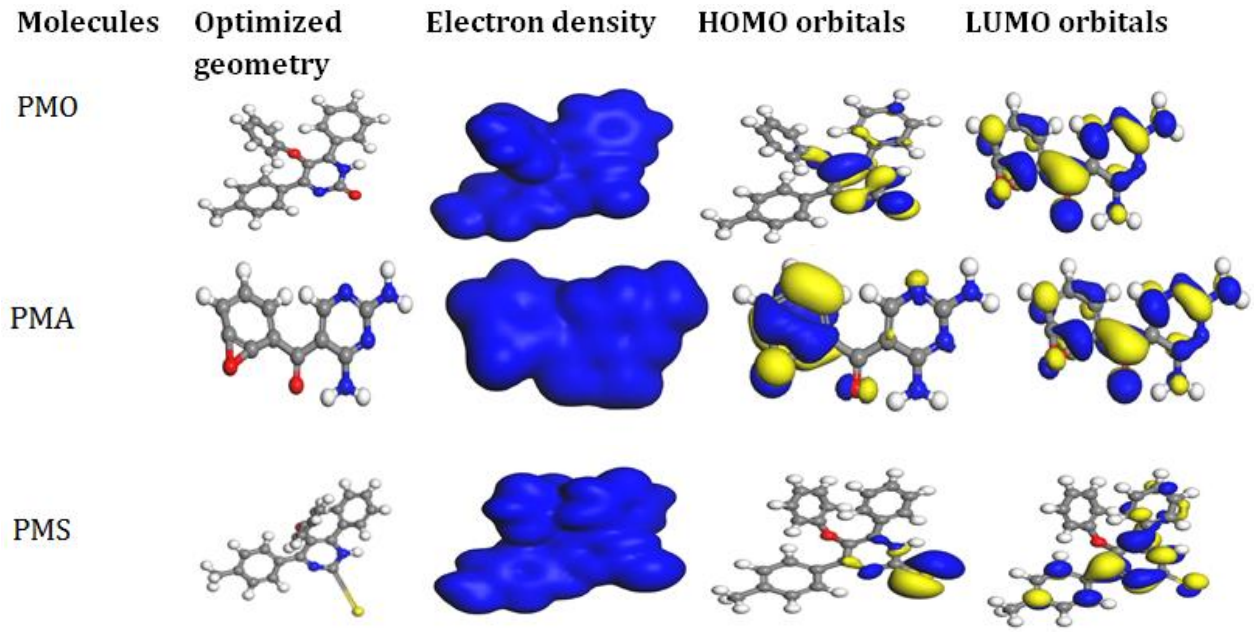

Fig. 2 Snapshot of the optimized electron density, HOMO and LUMO orbitals of the studied molecules

3-2-Quantum Chemical Properties

To get a better understanding of how molecules might interact with one another and exchange energy on the surface of a metal, quantum chemical parameters are examined. The energy of the highest occupied molecular orbital (E_{HOMO}) and the energy of the lowest unoccupied molecular orbital (E_{LUMO}) were used to derive the values for these quantum chemical parameters. Energy gap (ΔE), energy of back donation ($\Delta E_{b\text{-}d}$), electrophilicity index (ω), dipole moment (μ), electronegativity (χ), global hardness (η), global softness (σ), and proportion of electron(s) transfer (ΔN) are some of these metrics. The other two are electron receiving power (ω^+) and electron giving power (ω^-), respectively.

3-3-EHOMO, ELUMO and Energy gap (ΔE)

According to the factors examined, E_{HOMO} refers to a molecule's capacity to denote electrons from one electron-rich molecular orbital to the lowest unoccupied molecular orbital [16]. The ability of the molecule to donate or give away electrons to the metal surface during corrosion inhibition is strongly correlated with the value of E_{HOMO} [3-4]. According to the results of the study on pyrimidine derivative compounds, the PMS moiety has relatively the largest value of E_{HOMO}. As a result, the investigated inhibitors' E_{HOMO} values fell in the following order: PMS>PMA>PMO. Therefore, larger values of E_{HOMO} imply a better inclination toward electron donation, boosting the inhibitor's ability to bind to mild steel, and leading to improved inhibitory effectiveness.

The examined E_{LUMO} characteristics, which are similar to those reported elsewhere [13], are presented in Table 1 in the sequence PMA>PMO>PMS. This E_{LUMO}, which denotes an electron deficiency and demonstrates the ability to receive electrons from the d-orbital of the metal surface, is reported in the order PMA>PMO>PMS. With rising HOMO and falling LUMO energy values, the inhibitor's ability to attach to the metal surface increases. As a consequence of the inhibitor molecule's reactivity towards adsorption on metallic surfaces, ΔE is a crucial characteristic (physisorption and chemisorption). The findings in Table 1 demonstrated that the compound PMS has a lower ΔE and the stability of the inhibitor molecule toward adsorption on the metal surface is measured by this characteristic. The reactivity of the molecule increases as ΔE diminishes (PMA>PMO>PMS), increasing the inhibitory efficacy of the molecule. Because PMS has the smallest energy gap (ΔE), it may be more effective as a corrosion inhibitor [12, 17].

3-4-Dipole moment (μ)

Another crucial electrical characteristic that emerges from the non-uniform distribution of charges on various atoms in the molecule is the dipole moment. The adsorption between the chemical substance and the metal surface is likely increased by the low value of Debye. With an increase in μ, the energy of the deformability rises, making it harder for molecules to adsorb at iron (Fe) surfaces, reducing the contact area between molecules and iron surfaces, and diminishing inhibitors' ability to prevent corrosion. The pattern in Table 1 of this study is PMO>PMA>PMS, which makes PMS a better inhibitor on mild steel surface than other examined inhibitors [3, 11, 17].

3-5- Ionization energy (IE) and electron affinity (AE)

Fundamental descriptions of the chemical reactivity of atoms and molecules include ionization energy (IE) and electron affinity (AE). High stability and chemical inertness are indicated by high ionization energy, whereas high reactivity of the atoms and molecules is indicated by low ionization energy. The ionization energy trend listed in Table is as follows: PMO>PMA>PMS. When compared to other analysed compounds, PMS has a high reactivity and high inhibition efficiency, which are both indicated by its relatively low ionization energy. The other factors that were previously discussed and this one are in good agreement [3-4, 11-12, 14].

3-6-Global hardness (η) and softness (σ)

Two crucial characteristics that describe a given molecule's molecular stability and reactivity are global hardness (η) and softness (σ) [18]. It is obvious that chemical hardness primarily refers to the resistance to deformation or polarization of the electron cloud of the atoms, ions, or molecules under minor perturbations of

chemical reaction [11]. A soft molecule has a modest energy gap compared to a hard molecule's big energy gap. In the current study, PMS have a lower energy gap than other compounds studied due to their lower hardness value. In general, the inhibitor with the highest global softness value and the lowest global hardness value is anticipated to have the highest inhibitory efficiency [3-4, 11-12, 14]. Adsorption could take place in the region of the molecule where softness (σ), a local feature, has the largest value for the simplest electron transport [10]. The most effective inhibition occurs in PMS with the highest softness value. This trend is in line with the other previously mentioned characteristics.

3-7-Number of electrons transferred (ΔN)

Table 1 also includes the results of a calculation of the number of electrons transmitted (ΔN) from the inhibitor molecule to the iron metal. The calculated ΔN values demonstrate agreement between Lukovit's work and the inhibitory efficiency brought on by electron donation. Since ΔN values where all found to be less than 3.6, the inhibition efficiency of all the studied molecules increases by increasing their electron- donating ability to the metal surface. The ability of these inhibitors to donate electrons to the metal surface improves in the following order, PMS>PMO>PMA because of the increase in the obtained ΔN value. The findings show a substantial correlation between ΔN values and the previously mentioned parameters. Therefore, the relatively best inhibitor (PMS) with a value of ΔN = +2.448 has the highest fraction of electrons transmitted, whereas the inhibitor (PMA) with the lowest fraction can be regarded as the inhibitor with the lowest inhibitory efficiency [3-4, 11-12, 14].

3-8- The global electrophilicity index (ω) and Electronegativity (χ)

Parr developed the global electrophilicity index to quantify energy loss brought on by the greatest possible of electron flow between donor and acceptor entities. This index assesses the likelihood of chemical species to accept electrons, as stated in the Parr definition. Good electrophilic specie, on the one hand, is characterized by a high value of μ and low ω, while on the other hand good nucleophilic specie is characterized by a lower value of μ and high ω. This novel reactivity index calculates the energy stabilization when the system absorbs an extra electrical charge ΔN from the surrounding environment. The order of electronegativity (χ) in Table 1 is PMO>PMA>PMS. According to Sanderson's electronegativity equalization concept, PMOs with high electronegativity and low electronegativity differential (χ) fast attain equalization and as a result, poor reactivity is anticipated, which in turn predicts low inhibition efficiency. As a result, an increase in the electronegativity difference between the inhibitor and metal is indicated in the order PMS>PMA>PMO. This and the observations of other parameters earlier discussed are in strong agreement [3-4, 11-12, 14].

3-9- ΔEBack-donation

The charge transfer to a molecule, followed by a back-donation from the molecule, is energetically preferred when $\eta > 0$ and $\Delta E_{back\text{-}donation} < 0$. Since there will be a contact with the same iron metal in this context, it is therefore conceivable to compare the stability of inhibitory molecules, and it is anticipated that the charge transfer will decrease as the hardness increases. Calculated $\Delta E_{back\text{-}donation}$ values for the inhibitors reported in Table 1 demonstrate that they are occur in the following order: PMS>PMO>PMA, indicating that the best inhibitor, PMS, is given preference for energy of back-donation [11, 17]. This is in line with the other parameters observed in this work.

3-10- Electron donating (ω-) and accepting (ω+) powers

The stabilizing energy of a system as it becomes saturated with electrons from the environment is represented by the electrophilicity index (ω). Equation (12) defines the electron donating (ω^-) and Equation (13) indicates the electron receiving (ω^+) powers of species. As a result, a system with a higher ω^+ value will be better at receiving charge, whereas one with a lower value will be better for donating electrons. The net electrophilicity ($\Delta\omega^\pm$), which describes the electron accepting power in relation to the electron donating power, has been proposed to compare ω^+ with ω^- values. Table 1 provides the compounds' computed net electrophilicity ($\Delta\omega^\pm$), electron donating (ω^-), and electron receiving (ω^+) capabilities. The results from Table 1 clearly indicate that all the molecules are relatively electron donating in the order PMS>PMO>PMA based on the assumption of the validity of the Koopmans' theorem in DFT [19].

Table 1 Quantum parameters of the studied molecules

Inhibitors	PMO	PMA	PMS
E_{HOMO} (eV)	-4.910	-4.795	-3.911
E_{LUMO} (eV)	-2.320	-2.040	-2.325
ΔE (eV)	2.590	2.755	1.586
μ (debye)	3.615	3.417	3.118
IE (eV)	4.910	4.795	3.911
AE (eV)	2.320	2.040	2.325
χ (eV)	3.615	3.418	3.118
η (eV)	1.295	1.378	0.793
σ (eV)$^{-1}$	0.772	0.726	1.261
ΔN	1.307	1.300	2.448
ω (eV)	5.046	4.239	6.130
$\Delta E_{b\text{-}d}$ (eV)	-0.324	-0.345	-0.198
ε (eV)$^{-1}$	0.198	0.236	0.163
ω^- (eV)	7.015	6.120	7.788
ω^+ (eV)	3.400	2.703	4.700
$\Delta\omega^\pm$(eV)	10.415	8.823	12.488

3-11- Condensed Fukui function

Another crucial tool used to assess each atom's reactivity within the molecule is the Fukui function. The condensed Fukui function f^+ displays atoms with the highest propensity for nucleophilic attack, while f^- displays atoms with the highest propensity for electrophilic attack [20-21].

The condensed Hirshfield and Mulliken Fukui functions of the pyrimidine derivatives examined with the highest eigen values are presented in Table 2. Accordingly, the N(2) atom in the PMO molecule is in charge of the nucleophilic assault on the compound, whilst the O(7) atom is in charge of the electrophilic attack. In the case of PMA molecule, the oxygen atoms are in charge of both the nucleophilic attack at O(14) and the electrophilic attack at O(15). Due to the highest condensed Fukui function found on it in both Hirshfield and Mulliken values, the atom S(7) on the PMS molecule is discovered to be responsible for both nucleophilic and electrophilic attack [12].

To make it simple to identify the atoms in each molecule that are responsible for the reactivity and potential inhibition on the metal surface, Figure 3 displays the labelled atoms in each molecule. According to these molecules' figures, atoms in pyrimidine derivatives present can be identified through their structures' Mulliken and Hirshfied values [22].

The pyrimidine derivatives' maximal atom values suggest a larger likelihood of electron donation or acceptance from each of them [23]. The values of these atoms are shown in Table 2 of the examined compounds' Fukui orbitals.

Table 2 Fukui eigen values for the studied molecules

		Nucleophilic attack		**Electrophilic attack**	
Inhibitor	Atom	Mulliken	Hirshfield	Mulliken	Hirshfield
PMO	N(2)	0.080	0.069	0.073	0.063
	O(7)	0.068	0.063	0.168	0.162
PMA	O(14)	0.119	0.106	0.036	0.046
	O(15)	0.079	0.065	0.153	0.157
PMS	S(7)	0.161	0.131	0.466	0.441

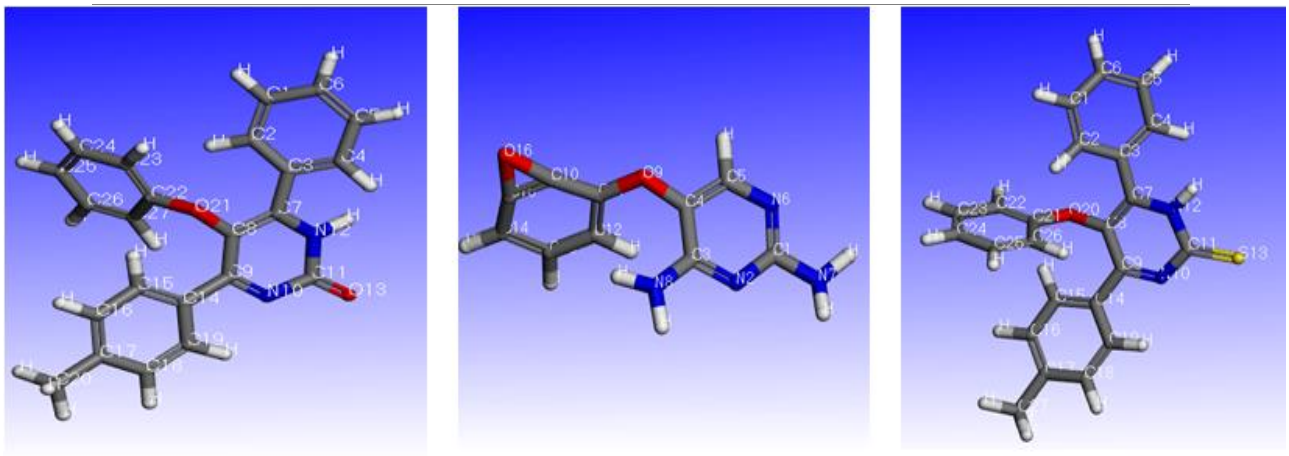

PMO **PMA** **PMS**

Fig. 3 The labelled atoms of the studied pyrimidine derivatives

3-12- Fukui Second function

A further local function of quantum mechanics is the Fukui second function, also referred to as the dual descriptor Δf(k). It is characterized by the distinction between nucleophilic and electrophilic Fukui functions, which also control the molecules' electrophilicity or nucleophilicity by utilizing their atoms' Fukui behavior. Site f(k) favours a nucleophilic assault if $f^2(r) > 0$, whereas site f(k) prefers an electrophilic attack if $f^2(r) < 0$. Accordingly, $f^2(r)$ can also be used to measure a molecule's selectivity for nucleophilic and electrophilic assaults [12]. According to the pyrimidine derivative results, the compounds exhibit potential for nucleophilic attack in the following order: PMO> PMA> PMS, as

demonstrated graphically in Figure 4. i.e. sending more electrons to the metal surface's d-orbital than they receive [12]. Thus, Table 3 indicates the percentage of nucleophilic, electrophilic and neutral characteristics of the studied molecules.

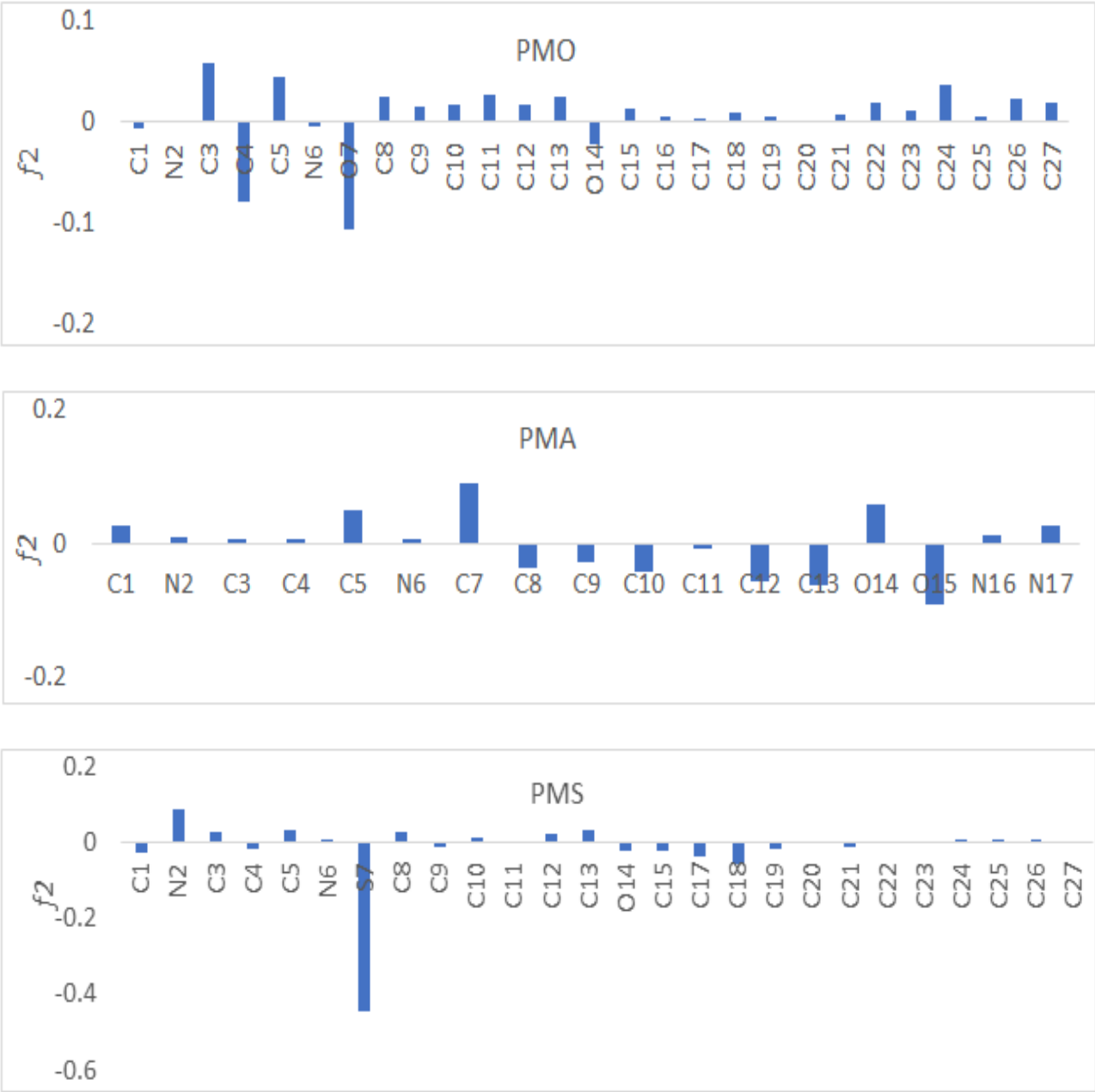

Fig. 4 Fukui second function graph of the analysis

Table 3 The percent second order Fukui function

Inhibitor	Nucleophilic (f^{2+})	Electrophilic (f^{2-})	Neutral
PMO	81.48	18.52	-
PMA	58.80	41.20	-
PMS	37.00	37.00	26.00

3-13-Molecular dynamics simulation

3-13-1- Adsorption orientation

To examine the nature of the interaction of the studied molecules on the surface of Fe (111) through Forcite quench dynamics, molecular dynamic simulations were run. When the system's energy was believed to be at its lowest, the total energy, the metal's surface energy, and the energy of the molecules were calculated [12]. Figure 5 depicts images of the top and side views of the pyrimidine derivatives' molecular interactions with the metal's surface. The figures make it abundantly evident that the molecules were adsorbed onto the surfaces of the metals, and that heteroatoms of nitrogen and oxygen are responsible for the interaction between the molecules and the metal surfaces. On the surface, each molecule was seen to maintain a parallel geometric orientation [24]. Higher inhibition efficacy is anticipated from the inhibitor's pyrimidine molecules based on the aforementioned observations.

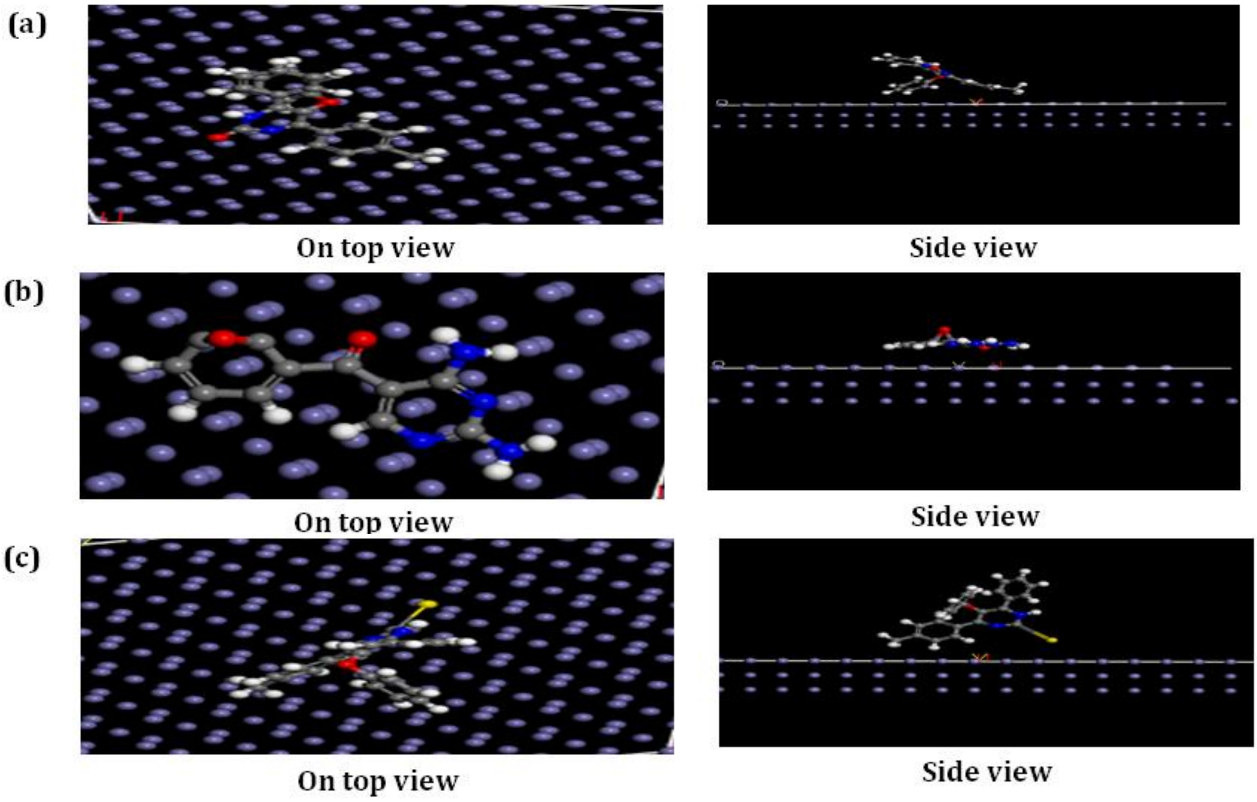

Figure 5 Snapshots of a) PMO, b) PMA, and c) PMS molecule onto the surface of Fe(111)

3-13-2- Adsorption bond angle

The optimized molecules with geometrically low energy were the molecules used for the bond angle computation before and after adsorption onto the surface of Fe (111) [11,17]. The nature and extent of the lowest energy molecule's interaction with the surface of Fe(111) metal were taken into account while calculating the bond angles of the molecules [17]. When the obtained angles before and after adsorption were compared, the results shown in Table 4 indicated that the majority of the angles lie within the trigonal planer (120°) orientation. A hint of the nature of the interaction between

metals and the molecule may be seen in the slight variations in bond angles between before and after the simulation process. These molecules are expected to exhibit sp^2 hybridization with higher p-character as a result of their geometric orientation on the surface of the metal [17].

Table 4 Bond angle of molecules before and after simulation

PMA			PMO			PMS		
Bond Angle(°)	Before Simulation	After Simulation	Bond Angle(°)	Before Simulation	After Simulation	Bond Angle(°)	Before Simulation	After Simulation
C1-N2-C3	117.4	117.1	N12-C11-N10	114.5	115.5	N12-C11-N10	115.9	114.5
N2-C1-N7	116.5	120.0	O13-C11-N10	125.9	115.9	S13-C11-N10	125.2	125.9
C1-N6-C5	117.8	110.0	C8-C11-N12	124.3	124.3	C8-C11-N12	124.3	124.3
N2-C3-N8	122.6	119.8	O13-C11-N12	119.6	119.6	S13-C11-N12	118.7	119.6
N8-C3-C4	117.9	119.9	C8-C21-C22	118.2	118.1	C8-C21-C22	117.2	118.2
C4-O9-C11	121.8	122.0	O21-C8-C7	115.8	115.9	O21-C8-C7	115.8	115.8
C15-O16-C10	53.8	56.3	N10-C9-C14	114.9	114.8	N10-C9-C14	115.9	114.9
			N12-C7-C3	116.3	116.1	N12-C7-C3	117.3	116.3

3-13-3- Adsorption bond length

The degree of interaction between the adsorbed molecule and the surface of the Fe(111) metal can be further determined by the length of the molecular bonds before and after interactions. The bond length, which measures the separation between the nuclei in a covalent connection, reveals the nature and strength of the covalency between the atoms [11,17]. Because of the type of molecule-Fe (111) interaction described in Table 5, there aren't many differences between the bond lengths of pyrimidine molecules after and before simulation. All of the bonds in the molecule PMA and PMS undergo modifications, demonstrating that every component of the molecule was utilized throughout the simulation on the surface. Due to the nature of the interaction between the surface and the molecule in PMO, no changes in the bond lengths of C9-C14, C9-C14, or C7-C3 were observed. This is a clear sign that the molecules' interaction with the metal's surface was not very pronounced [17].

Table 5 Bond length of molecules before and after simulation

PMA			PMO			PMS		
Bond Length (Å)	**Before Simulation**	**After Simulation**	**Bond Length (Å)**	**Before Simulation**	**After Simulation**	**Bond Length (Å)**	**Before Simulation**	**After Simulation**
			O13-C11	1.246	1.236			
C1-N2	1.332	1.322	C11-N10	1.370	1.377	S13-C11	1.647	1.673
N2-C3	1.367	1.356	C11-N12	1.422	1.400	C11-N10	1.349	1.344
C3-C4	1.472	1.400	N12-C7	1.360	1.365	C11-N12	1.391	1.390
C4-C5	1.362	1.332	N10-C9	1.331	1.322	N12-C7	1.345	1.345
C5-N6	1.325	1.365	C8-O21	1.398	1.399	N10-C9	1.315	1.353
C1-N7	1.359	1.366	O21-C22	1.403	1.423	C8-O20	1.363	1.366
C4-O9	1.378	1.317	C9-C14	1.467	1.467	O20-C22	1.365	1.365
O9-C11	1.331	1.421	C22-C23	1.385	1.449	C9-C14	1.463	1.466
C11-C12	1.411	1.444	C9-C14	1.469	1.469	C22-C23	1.379	1.377
C12-C13	1.420	1.200	C7-C3	1.456	1.456	C9-C14	1.463	1.460
C13-C14	1.224	1.300				C7-C3	1.453	1.444
C14-C15	1.324	1.421						
C15-O16	1.435	1.411						
O16-C10	1.464	1.424						
C10-C11	1.321	1.312						

3-13-4- Adsorption and binding energies

According to results reported in Table 6, the calculated adsorption energies of the compounds under study for PMA, PMS, and PMO are: -34.96 kcalmol^{-1}, -60.65 kcalmol^{-1}, and -42.66 kcalmol^{-1}, respectively. Strong molecular adsorption on the surface of Fe (111) is responsible for lower adsorption energy values or higher binding energies [25]. According to the computed values in Table 6, the binding or adsorption energies are all less than $\pm$100 kcalmol^{-1}, which John *et al.* [16] stated as the cutoff point for the values of adsorption in their respective investigations. On the surface of metals during simulation, these values distinguish between physical and chemical adsorption; -100 kcalmol^{-1} for adsorption energy and +100 kcalmol^{-1} for binding energy [13]. The binding energy of the moieties increase was in the order of PMS> PMO> PMA which agreed with observed order of inhibition established for previous quantum chemical parameters analysed.

Table 6 Adsorption Parameters for the interaction of the studied molecules with the Fe (111) surface

Properties	**Molecules**		
	PMA	PMS	PMO
Total potential energy (kcalmol^{-1})	-101.46	107.54	-102.73
Energy of the molecule (kcalmol^{-1})	-66.78	168.19	-60.059
Energy of the Fe(111) (kcalmol^{-1})	0.000	0.0000	0.0000
Adsorption energy (kcalmol^{-1})	-34.96	-60.65	-42.66
Binding energy (kcalmol^{-1})	34.69	60.65	42.66

4- Conclusion

Density functional theory (DFT) was used to evaluate the quantum chemical parameters of the three optimized pyrimidine derivatives in relation to their adsorption on Fe(1 1 1) metals surface. Both global and local reactivity indices evaluated showed that the molecules are all potential corrosion inhibitors on Fe(1 1 1) surface in the order PMS>PMO>PMA. The assessed Fukui indices of the studied molecules showed that they are more nucleophilic than electrophilic in nature with their hetero atoms as source of electron donating entities. The assessment of molecules bond lengths and angles proved that the nature of the interaction between the pyrimidine derivatives and the Fe(1 1 1) surface is through adsorption with an sp^2 (trigonal) orientation. The use of the quenched molecular dynamic simulation to ascertain the nature and strength of interaction of the pyrimidine derivatives with the Fe(1 1 1) surface prove them to obey the mechanism of physical adsorption based on the evaluated adsorption and binding energy values.

Conflict of interest

The authors declare no conflict of interest.

Acknowledgments

The authors are grateful to Dr. Arthur Ebuka David, Department of Pure and Applied Chemistry, University of Maiduguri, Borno State, Nigeria for the BIOVIA Materials Studio software installation.

References

[1] H. A. Al Mashhadani and K. A. Saleh, Electrochemical Deposition of Hydroxyapatite Co-Substituted By Sr/Mg Coating on Ti-6Al-4V ELI Dental Alloy Post-MAO as Anti-Corrosion", *Iraqi Journal of Science*, 61,(2020) 2751–2761.

[2] L. Afandiyeva, V. Abbasov, L. Aliyeva, S. Ahmadbayova, E. Azizbeyli, and HM. El-Lateef Ahmed, Investigation of organic complexes of imidazolines based on synthetic oxy-and petroleum acids as corrosion inhibitors, *Iranian Journal of Chemistry and Chemical Engineering (IJCCE)*, 37(2018) 73-90.

[3] H. Jafari, F. Mohsenifar, and K. Sayin, Effect of alkyl chain length on adsorption behavior and corrosion inhibition of imidazoline inhibitors, *Iranian Journal of Chemistry and Chemical Engineering (IJCCE),* 37, (2018) 85-103. https://doi.org/10.30492/ijcce.2018.29779.

[4] S. Elmi, MM. Foroughi, M. Dehdab, and M. Shahidi-Zandi, "Computational evaluation of corrosion inhibition of four quinoline derivatives on carbon steel in aqueous phase", *Iranian Journal of Chemistry and Chemical Engineering (IJCCE),* 38, (2019) 185-200.

[5] BN. Noorollahy, HR. Hafizi-Atabak, F. Atabaki, M. Radvar, and S. Jahangiri, "Electrochemical measurements for the corrosion inhibition of mild steel in 0.5M HCl using poly (epichlorohydrin) derivatives", *Iranian Journal of Chemistry and Chemical Engineering (IJCCE),* 39 (2020) 113-25.

[6] LT. Popoola, TA. Aderibigbe, and MA. Lala, "Mild steel corrosion inhibition in hydrochloric acid using cocoa pod husk-ficus exasperata: extract preparation optimization and characterization" *Iranian Journal of Chemistry and Chemical Engineering (IJCCE)*, 41(2022) 482-92.

[7] R. M. Kubba and N. M. Al-Joborry, Theoretical study of a new oxazolidine -5- one derivative as a corrosion inhibitor for carbon steel surface, *Iraqi Journal of Science*, 62, (2021) 1396–1403.

[8] K. A. K. Al-Rudaini and K. A. S. Al-Saadie, Milk Thistle Leaves Aqueous Extract as a New Corrosion Inhibitor for Aluminum Alloys in

Alkaline Medium", *Iraqi Journal of Science*, 62 (2021)363–372.

[9] M. A. Mohammed and R. M. Kubba, Experimental Evaluation for the Inhibition of Carbon Steel Corrosion in Salt and Acid Media by New Derivative of Quinolin-2-One, *Iraqi Journal of Science*, 61 (2020) 1861–1873.

[10] S. Mammeri, N. Chafai, H. Harkat, R. Kerkour, and S. Chafaa, Protection of steel against corrosion in acid medium using dihydropyrimidinone derivatives: experimental and DFT study, *Iranian Journal of Science and Technology, Transactions A: Science*, 45, (2021) 1607-19.

[11] TV. Kumar, J. Makangara, C. Laxmikanth, and NS. Babu, Computational studies for inhibitory action of 2-mercapto-1-methylimidazole tautomers on steel using of density functional theory method (DFT), *International Journal of Computational and Theoretical Chemistry,* 4 (2016)1-6.

[12] TO. Esan, OE. Oyeneyin, A. Deola, and NI. Olanipekun, Corrosion inhibitive potentials of some amino acid derivatives of 1, 4-naphthoquinone– DFT calculations, *Advanced Journal of Chemistry-Section A*, 5(2022) 263-270.

[13] R. M. Kubba, N. M. Al-Joborry, and N. J. Al-lami, Theoretical and Experimental Studies for Inhibition Potentials of Imidazolidine 4-One and Oxazolidine 5-One Derivatives for the Corrosion of Carbon Steel in Sea Water, *Iraqi Journal of Science*, vol. 61 (2020) 2776–2796.

[14] Z. Yavari, M. Darijani, and M. Dehdab, Comparative theoretical and experimental studies on corrosion inhibition of aluminum in acidic media by the antibiotics drugs, *Iranian Journal of Science and Technology, Transactions A: Science,* 42 (2018) 1957-67.

[15] N. M. Al-Joborry and R. M. Kubba, Theoretical and Experimental Study for Corrosion Inhibition of Carbon Steel in Salty and Acidic Media by A New Derivative of Imidazolidine 4-One, *Iraqi Journal of Science*, 61(2020) 1842–1860.

[16] S. John, J. Joy, M. Prajila, and A. Joseph, Electrochemical, quantum chemical, and molecular dynamics studies on the interaction of 4-amino-4H, 3, 5-di (methoxy)-1, 2, 4-triazole (ATD), BATD, and DBATD on copper metal in $1NH_2SO_4$, *Materials and Corrosion,* 62 (2011) 1031-41.

[17] ME. Belghiti, S. Echihi, A. Dafali, Y. Karzazi, M. Bakasse, H. Elalaoui-Elabdallaoui, LO. Olasunkanmi, EE. Ebenso, and M. Tabyaoui, Computational simulation and statistical analysis on the relationship between corrosion inhibition efficiency and molecular structure of some hydrazine derivatives in phosphoric acid on mild steel surface, *Applied Surface Science*, 491 (2019) 707-22.

[18] M. M. Kadhim, L. A. A. Juber, and A. S. M. Al-Janabi, Estimation of the Efficiency of Corrosion Inhibition by Zn-Dithiocarbamate Complexes: a Theoretical Study", *Iraqi Journal of Science,* 62 (2021) 3323–3335.

[19] D. Glossman-Mitnik, Computational study of the chemical reactivity properties of the rhodamine B molecule, international conference on computational science, ICCS, *Procedia Computer Science,* 18 (2013) 816 – 825.

[20] A. Nahlé, R. Salim, F. El Hajjaji, MR. Aouad, M. Messali, E. Ech-Chihbi, B. Hammouti, and M. Taleb, Novel triazole derivatives as ecological corrosion inhibitors for mild steel in 1.0 M HCl: experimental & theoretical approach, *RSC advances,* 11(2021) 4147-62.

[21] NO. Eddy, PO. Ameh, and NB. Essien, Experimental and computational chemistry studies on the inhibition of aluminium and mild steel in 0.1 M HCl by 3-nitrobenzoic acid, *Journal of Taibah University for Science,* 12 (2018) 545-56.

[22] L. Guo, M. Zhu, J. Chang, R. Thomas, R. Zhang, P. Wang, X. Zheng, Y. Lin, and R. Marzouki, Corrosion inhibition of N80 steel

by newly synthesized imidazoline based ionic liquid in 15% HCl medium: experimental and theoretical investigations, *Int. J. Electrochem. Sci*., 16 (2021) 211139-2.

[23] H. Lgaz, S. Masroor, M. Chafiq, M. Damej, A. Brahmia, R. Salghi, M. Benmessaoud, IH. Ali, MM. Alghamdi, A. Chaouiki, and IM. Chung, Evaluation of 2-mercaptobenzimidazole derivatives as corrosion inhibitors for mild steel in hydrochloric acid, *Metals*, 10 (2020) 357-69.

[24] F. Iorhuna, NA Thomas, SM Lawal. Theoretical properties of Thiazepine and its derivatives on inhibition of Aluminium *Al (110)* surface*. Alger. J. Eng. Technol.,* 8 (*2023*)43-51.

[25] G. Kılınççeker, M. Baş, F. Zarifi, and K. Sayın, Experimental and computational investigation for (E)-2-hydroxy-5-(2-benzylidene) aminobenzoic acid schiff base as a corrosion inhibitor for copper in acidic media, *Iranian Journal of Science and Technology, Transactions A: Science,* 45 (2021)515-27, 2021.

[26] T. A. Nyijime , H.F. Chahul, A. M. Ayuba, F. Iorhuna. Theoretical Investigations on Thiadiazole Derivatives as Corrosion Inhibitors on Mild Steel. *Adv. J. Chem. A*, 6(2023), 141-154.

[27] O. O Emmanuel, O. B. Samuel, O. F. Kolawole, A. D. Dada, A. E. Oluwafisayo, E. B. Chibuzo, I. Nureni, Experimental and Theoretical Study on the Corrosion Inhibitive Potentials of Schiff Base of Aniline and Salicyaldehyde on mild steel in 0.5M HCl, *Ad. J. Chem. B,* 2 (2020) 197-208

HOW TO CITE THIS ARTICLE

Fater Iorhuna, Abdullahi Muhammad Ayuba, Abdulfatah Shehu Muhammad. Computational Studies on the Corrosion Inhibition of Mild Steel Using Pyrimidine Derivatives, Adv. J. Chem. B, 5(2023) 244-260.

DOI: 10.48309/ajcb.2023.398019.1173

URL: https://www.ajchem-b.com/article_176317.html